A shared PV system for transportation and residential loads to reduce curtailment and the need for storage systems

Diab, Ibrahim; Damianakis, Nikolaos; Chandra-Mouli, Gautham Ram; Bauer, Pavol

Important note
To cite this publication, please use the final published version (if applicable).
Please check the document version above.

A shared PV system for transportation and residential loads to reduce curtailment and the need for storage systems☆

Ibrahim Diab *, Nikolaos Damianakis, Gautham Ram Chandra-Mouli, Pavol Bauer

Technische Universiteit Delft (TU Delft), Faculty of Electrical Engineering, Mathematics, and Computer Science, Electrical Sustainable Energy Department, Mekelweg 4, 2628 CD Delft, The Netherlands

ARTICLE INFO

ABSTRACT

This paper proposes a shared multi-stakeholder PV system for traction substations and nearby residential loads to reduce the need for storage, AC grid exchange, and curtailment. The residential stakeholders offer both the base electrical load and the solar panels installation space needed by the traction stakeholder, who brings the peak load and investments to the former.

Two case studies were conducted for one year in the city of Arnhem, The cy=Netherlands, using comprehensive and verified simulation models: A high-traffic and a low-traffic substation. The results showed a positive, synergetic benefit in reducing the PV system's excess energy and size requirement for any type of traction substations connected to any number of households.

In one detailed example, the multi-stakeholder system suggested in this paper is shown to reduce curtailment by up to 80% in moments of zero-traction load. Generally, the direct load coverage of a PV system is increased by as much as 7 absolute percentage points to the single-stakeholder system when looking at energy-neutral system sizes. This multi-stakeholders system offers then an increase in the techno-economic feasibility of PV system integration in urban loads.

1. Introduction

Renewable energy systems like solar photovoltaic (PV) offer scalable, decentralized, and sustainable power supply at increasingly competitive costs [1]. However, their intermittent generation profile creates a major hurdle for their techno-economic feasibility. This is because the power mismatch between this generation and the connected load requires storage systems and/or exchange with the main city grid (when allowed). In more practical choices, the most economical option is to curtail the excess power. These options are illustrated in Fig. 1.

The first solution of using storage systems is high in both losses (transmission, self-discharge, battery efficiency, etc.) and system costs. Meanwhile, for the second solution of using the local, the grid requirements impose strict export limitations on the power sent to the AC grid – if allowed at all – to maintain the stability and controllability of the grid. Finally, curtailment directly influences the effective energy cost of the PV system and, in environments where the available space for PV implementation is already limited, can jeopardize the techno-economic feasibility of the project or its implemented scale.

Consequently, it is in the techno-economic interest of the PV system stakeholders to increase the direct utilization of their PV system output

by the load. However, matching demand and generation is a different challenge depending on the type of load profile. Below are two examples of such profiles: Urban traction loads and residential dwellings loads.

1.1. Challenges for PV system integration in urban traction grids

Catenary traction grids like trams or trolleybus are segmented into substations that consist of a step-down transformer and a rectifier that turns the Low Voltage AC to a Low Voltage DC at about 650-750V, depending on the traction substation and the trolley city.

The load profile of such traction networks is particular in two aspects. First, the load is stochastic and unpredictable both in time and location since the vehicles are moving with the city traffic [2,3]. Second, when the vehicle exits the supply zone of one substation and enters another, the load suddenly disappears from the first substation. In that sense, traction grids are particular grids with no base loads and with high, unpredictable power peaks caused by vehicle acceleration (about five times that of cruising traction [4–6]).

Previous works in the literature [7–9] have proven that the direct utilization of an energy-neutral sized, traction-substation-connected PV

---

* Corresponding author.
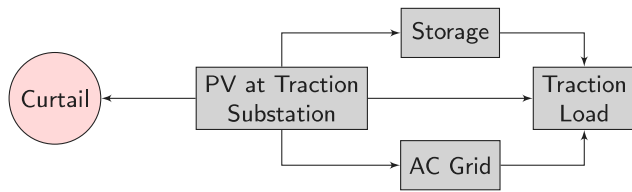*E-mail address:* i.diab@tudelft.nl (I. Diab).

Fig. 1. Generated PV energy can be used directly by the Traction Load (most desirable), stored for later traction use, exchanged with the AC Grid, or curtailed (wasted).

system (Fig. 2) can be as low as 13% in low-traffic substations, and quickly reaches a plateau of about 38% with busier substations. This means that if the excess generation is curtailed, less than 40% of the PV energy is used from a system that was sized to feed 100% of the load. The effective energy cost is thereby more than 2.5 times higher than that of the installed capacity. If the system is undersized to reduce the absolute amount of energy wasted, less of the traction load is covered. Other works have also shown the sizing limitation of a traction-grid-connected PV system because of the load and generation mismatch [10].

This has motivated calls in the literature for the integration of more base loads into traction networks [8,9,11–13].

1.2. Challenges for PV system integration for urban electrified household demands

The residential sector is one of the most significant users of energy, accounting for about a quarter of total global energy use [14].

In an effort to decarbonize this load sector, its heating and transportation demands are increasingly electrified in the form of Heat Pumps (HPs) and private Electric Vehicles (EVs) [15].

However, a challenge with coupling PVs and HPs is that the higher periods of PV generation occur when the buildings are not occupied and the HPs are not in their periods of higher demand. Therefore, energy storage and demand response are necessary for PV rooftops with minimum grid power exchange [16,17].

However, the simultaneous installation of energy storage, heat pumps, and PV panels can be costly for a household and demotivate projects of demand electrification.

1.3. Advantages of a shared PV infrastructure for transport and residential loads (this paper)

The challenges and opportunities of PV integration in either transport or residential networks are complementary to each other. In the case of the former, there is an absence of a base load during the day, yet power peaks occur frequently and during daylight hours. In the latter's case, a base load is present, yet not enough load peaks occur during the higher PV generation periods.

Therefore, there is an expected synergy in coupling traction substations and nearby residential loads in increasing the overall matching between load and generation.

Furthermore, rooftop PV systems can offer physical installation space otherwise, which is otherwise scarcely available in urban environments for the transport grids.

This suggestion is illustrated in Fig. 3, where traction grids such as trolleybus grids that are fed from the LVAC network can aggregate their load demand with that of nearby residential homes. This aggregated load can be served by rooftop PV systems. It is important to point out that there is no active load control in this method, but rather a bundling of stakeholders for a scenario somewhat equivalent to an on-site Power Purchase Agreement with solar assets (see [18] for the example of Dutch railways and wind power).
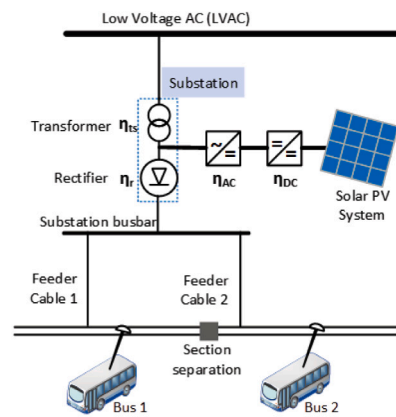

Fig. 2. The PV-powered trolleygrid and its components. Here, the PV is connected to the AC side to avoid installing costly storage systems for the excess PV energy.
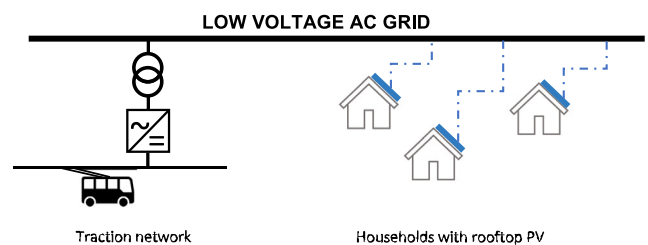

Fig. 3. The suggested multistakeholder in this paper: Traction substations like trolleybuses and nearby households can form one load entity via the Low Voltage AC grid to reduce the need for energy storage.

1.4. Paper contributions

This paper offers the following contributions:

1. The proposition for how to integrate residential PV systems with transport grids to create a multi-stakeholder renewable energy generation and transport system
2. A detailed study of the decrease in the need for storage, MVAC grid exchange, and/or curtailment for the proposed multi-stake holder PV system using comprehensive and verified trolleybus, trolleygrid, heat pump, and PV models for one year with a per-second resolution
3. A detailed study of the increase in the direct load coverage out of an effective PV system size in the proposed multi-stake holder PV system case using comprehensive and verified trolleybus, trolleygrid, heat pump, and PV models for one year with a per-second resolution

1.5. Paper structure

In the following sections, the paper will first detail the case study methodology and modeling techniques in Section 2. Then, Section 3 offers the results of the benefits for the direct PV Utilization (PV and Load matching) of the combined system. Section 4 looks at the benefits for the load coverage of the combined system according to the share of each stakeholder. Finally, Section 5 closes with conclusions and recommendations.

2. Modeling methodology

2.1. Case study definition

There is a difference in the performance of a PV system connected to a traction substation depending on the length of the catenary that
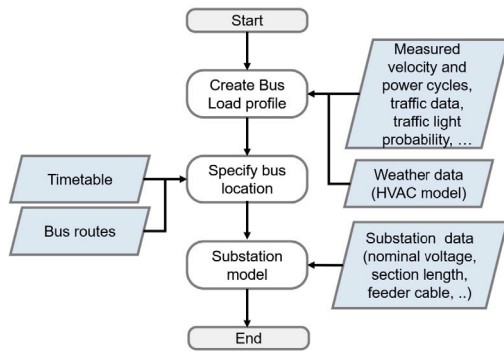
Fig. 4. Flowchart of the trolleybus grid model.

it supplies and on the average traffic that it observes [7,8]. For this purpose, this paper needs to confirm the benefit of the shared PV system by looking at at least two traction substation types. The examined trolleygrid is that of the city of Arnhem, The Netherlands.

For this paper, the choice is for:

- Substation 9 (SS9): A relatively short (less than 1000 m) catenary zone with up to 5 buses at a time in traffic density
- Substation 12 (SS12): A relatively long (more than 2000 m) catenary zone at most 3 buses at a time in traffic density

To study these grids, the simulations are run per second for a full year of operation. The PV systems, expected to primarily be rooftop systems, first supply the residential loads (closest) and then send the remaining energy through the LVAC connection to the nearby traction loads. The total losses are around 4.5% as derived in [8].

2.2. Trolleybuses and trolleygrids modeling

For the modeling of the trolleygrid and trolleybuses, this paper follows the flowchart described in Fig. 4, which uses:

- Verified traction and auxiliaries bus demands and velocities, of 1-second resolution, for a full year of trolley operation (detailed [4,7])
- A bus scheduling extrapolated from the bus timetables as well as delay probabilities to account for the stochastic nature of the bus position (detailed in [4])
- A comprehensive and verified nodal grid model (Fig. 4) that calculates, among other parameters, the minimum line voltage and maximum substation power demand (detailed in [4]), as opposed to the traditional energy approach or current-source modeling approaches found in the modeling literature as reviewed in [4,9]

Important features of this grid model are that it accounts for bilateral connections and feeder cables.

Another highlight of the model is that it models both the braking energy and the auxiliary demand of the trolleybus (mainly the heating and ventilation), which can be up to 50% of the bus power demand in harsh weather conditions [4,7,19]. The bus powers are given by Eq. (1). During braking, the bus power, P_{bus}, is the auxiliaries power P_{aux} plus the net exchanged with the grid P_{net} (obtained iteratively from the power flow calculation). The excess power, P_{BR}, is wasted in the braking resistors as demonstrated in Eq. (1).

While in traction mode, the bus power is simply the traction P_{tr} and the auxiliaries demand, P_{aux}.

$$P_{bus,j} = \begin{cases} P_{net,j} + P_{aux,j} + P_{BR,j} & \text{if braking} \\ P_{tr,j} + P_{aux,j} & \text{if traction} \end{cases} \quad j = 1..N_{bus} \tag{1}$$

The auxiliaries are -predominately- the HVAC load plus other base loads such as the on-board lights, screens, door motors, the control systems, etc.:

$$P_{aux} = P_{HVAC} + P_{base} \tag{2}$$

The HVAC energy requirement is calculated by a thermodynamic heat exchange model between the trolleybus and its surrounding environment and is detailed in [4].

From this energy requirement, the HVAC power is derived. For the Arnhem bus types, the HVAC system is controlled with a duty cycle (t_{cycle}) of 5 min. The on-time, t_{on}, of the HVAC system for each period is dictated by the HVAC energy requirement during that cycle:

$$t_{on} = t_{cycle} \frac{\overline{P_{HVAC}}}{P_{rated}} \tag{3}$$

where $\overline{P_{HVAC}}$ is the average power requirement in the 5 min and P_{rated} is the nominal HVAC power, namely 36.5 kW for the Arnhem system. Finally, in this paper, P_{base} is taken as 5 kW as an estimate provided from the Arnhem trolleybus measurements [4,19].

The nodal model is based on the forward–backward sweep convergence logic, where each load (trolleybus or EV charger) is considered a node. The model's output is, among others, the voltage and power at every node, the branch currents, and the losses. This provides the data needed for the detailed analysis of the grid violations.

The braking energy is treated as follows: First, the model runs until power-balance convergence. Second, the model checks to see if the substation current solution is a negative number (excess braking energy) and/or if the bus voltage is above the braking resistor limit (740V for Arnhem). If so, the regenerative bus power is curtailed by the "unacceptable" power amount, which is the substation voltage times the negative current and/or the bus voltage above 740 times the bus current. Then, the iteration is repeated, and this process, in general, is repeated until the results are acceptable. This is admittedly a slow convergence method where the curtailment is in the order of a few kWs at each step. Still, it robustly approaches the actually used bus power without overshooting it since the non-linearity of the power flow makes it hard to directly estimate the used braking energy and transmission losses from an analytical power balance. The only computationally-fast exception is when a braking bus is alone on the section (no load), so all the braking energy is immediately wasted.

2.3. PV power output model

The PV model is a per-second simulation of the energy output of the solar panels. The model takes into accounts parameters such as solar altitude (a_S), solar azimuth (A_S), global horizontal irradiance (GHI), diffuse horizontal irradiance (DHI), ambient temperature, ground temperature, and wind speed, among other. These values are obtained from Meteonorm [20] for one year, but forecast methods also exist (such as [21,22]) to predict future profiles.

The optimal azimuth angle and the tilt angle of the PV module are identified by iteration, in which the yearly irradiance per square meter on the module is calculated for each possible combination of azimuth and tilt. At these positions, the global irradiance, G_M, on the model is:

$$G_M = G_{M,dir} + G_{M,diff} + G_{M,refl} \tag{4}$$

Where the terms on the right-hand side are the direct, diffuse, and reflected irradiance on the tilted module, respectively. The detailed equations for these terms are described in [23]. The PV module efficiency is a function of the module's temperature. This temperature is estimated as a function of meteorological parameters using a Fluid Dynamic model. The model is based on the energy balance between the PV module and the external surroundings, accounting for convection,

Table 1
Building surfaces specifications used in this paper.

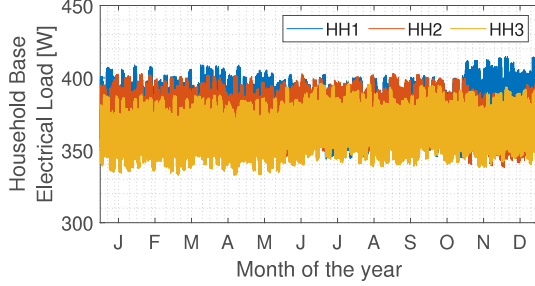| Surface (surf)	Material	Area A (m²)	Thickness d (m)	Conductivity U (W/mK)
Floor (fl)	Wood	90	0.03	0.18
Front/Back Walls (fw/bw)	Brick	15 × 5	0.23	1
Side Walls (sw)	Brick	6 × 8	0.23	1
Roof (rf)	Clay	15 × 4.25	0.015	0.72

Fig. 5. The three household load profiles used in this study based on publicly available data on the electricity demand of Dutch private dwellings [24].

conduction, and radiation heat transfers. The module's temperature, T_M, can be described as:

$$T_M = \frac{(1 - R)(1 - \eta)G_M + h_c T_a + h_{r,sky} T_{sky} + h_{r,gr} T_{gr}}{h_c + h_{r,sky} + h_{r,gr}} \quad (5)$$

Where R is the module reflectivity, η is the module's efficiency, h_c is the overall convective heat transfer coefficient (considering both top and back of the module), and T_a, T_{sky}, and T_{gr}, are the ambient, sky, and ground temperature, respectively. Finally, $h_{r,sky}$ and $h_{r,gr}$ are the linearized radiation heat transfer coefficient between the module and the sky and between the module and the ground, respectively. The PV module data sheet provided by the manufacturer shows the effect on the efficiency by the deviation of the solar cell temperature from standard testing conditions (STC).

However, quantifying the effect of irradiance variation on solar cell performance is less straightforward. The overall module efficiency accounting for both temperature and irradiance influence can be approximated as

$$\eta(T_M, G_M) = \eta(25\ °C, G_M)\left[1 + \kappa\left(T_M - 25\ °C\right)\right] \quad (6)$$

where the first term represents the effect of irradiance and the second that of temperature, with κ computed as:

$$\kappa = \frac{1}{\eta(STC)}\frac{\partial\eta}{\partial T} \quad (7)$$

and representing the temperature effect on the performance relative to the STC conditions efficiency [23].

The selected PV module is the 'AstroSemi 365W' mono-crystalline panels from Astroenergy. The solar modules have a 365 W_p rated power and a 19.7% efficiency at STC.

2.4. Household demand modeling: Electric loads and heating

2.4.1. Electric loads

The electric loads of the households have been modeled with the use of Probability Distribution Function (PDF) electricity profiles for the Netherlands of 2021. These profiles are downloaded from the NEDU open database [25], and they are categorized into E1 A and E1B for the residential sector. The E1 A profiles are generated with the use of only the day-meter, whereas also a night meter is used for the generation of the E1B.

Three final consumption profiles of a household are calculated by scaling its estimated yearly consumption PDF, as depicted in Fig. 5.

2.4.2. Heating demand model

The heating model includes mainly the building, space heating & domestic hot water (DHW), insulation, and power consumption models. The model is based on [26] which will be briefly explained as follows.

Regarding the building model, the typical Dutch terraced building type has been selected since it represents more than 50% of Dutch households. The building surfaces specifications (dimensions, materials, and conductivity values) are summarized in Table 1.

$$T_{bw}(t + \Delta t) = \frac{\dot{Q}_{gain}(t) - \dot{Q}_{los}(t)}{C_{tot}}\Delta t + T_b(t) \quad (8)$$

where:

$$C_{tot,b} = C_b + V_b C_{air}\rho_{air}\ \&\ C_{tot,w} = V_{tank}\ C_{wat}\ \rho_{wat} \quad (9)$$

$$\dot{Q}_{gain,b}(t) = \dot{Q}_{hp}(t) + \dot{Q}_{ir}(t)\ \&\ \dot{Q}_{gain,w}(t) = \dot{Q}_{hp}(t) \quad (10)$$

$$\dot{Q}_{ir}(t) = G_{inc}(t)\ w_b\ s_b \quad (11)$$

$$\dot{Q}_{los}(t) = \dot{Q}_{cond}(t) + \dot{Q}_{vent}(t) \quad (12)$$

$$\dot{Q}_{cond,b}(t) = \sum_{surf}^{surfaces}(d_{surf}U_{surf}A_{surf})(T_b(t) - T_a(t)) \quad (13)$$

$$\dot{Q}_{cond,w}(t) = U_{tank}A_{tank}(T_{tank}(t) - T_a(t)) \quad (14)$$

$$\dot{Q}_{vent}(t) = C_{air}\ \rho_{air}\ r_b(T_b(t) - T_a(t)) \quad (15)$$

Regarding the space & DHW heating/cooling model, Eq. (8) dictates that the temperature of the next timestep for both the building and the DHW tank depends on the total heat gains $\dot{Q}_{gain}$ & losses $\dot{Q}_{los}$ as well as the total heating capacity C_{tot}. According to (9), the total building capacity C_{tot_b} is the sum of the building heating capacity itself C_b and the capacity of the air inside, while the total DHW tank capacity is the capacity of the total water stored C_{tot_w}. The heating gains of the DHW tank $\dot{Q}_{gain,w}$ is the HP output $\dot{Q}_{hp}$, while for the building, the gained heat by irradiation is also included $\dot{Q}_{ir}$, as dictated by (10). According to (11), $\dot{Q}_{ir}$ depends on the total incident building irradiation G_{inc}, the building window-to-wall ratio w_b & the solar heat gain coefficient s_b. Eq. (12) shows that the total heating losses $\dot{Q}_{los}$ are the sum of the conduction losses $\dot{Q}_{cond}$ and the ventilation losses $\dot{Q}_{vent}$, which for the building are modeled in (13) & (15), respectively. The DHW tank losses $\dot{Q}_{cond,w}$ are only conductive and are modeled in (14)).

$$U_{des} = \frac{1}{\frac{d_{surf}}{U'_{surf}} + \frac{d_{ins}}{U'_{ins}}} \quad (16)$$

Regarding the insulation model, the walls and roof of the buildings are insulated according to (16). With use of 80 mm Expanded Polystyrene (EPS) of U = 0.024 W/mK & 110 mm PIR Board (Celotex) of U = 0.019 W/mK, the walls and roof conductivities U'_{walls} & U'_{roof} have been decreased to comply with the new regulations (0.28 W/m²K & 0.17 W/m²K, respectively). It is then assumed here that the buildings in the future are well insulated, and floor heating using a heat pump would be sufficient.

$$P_{hp}(t) = \frac{\dot{Q}_{hp}(t)}{COP(t)} \quad (17)$$

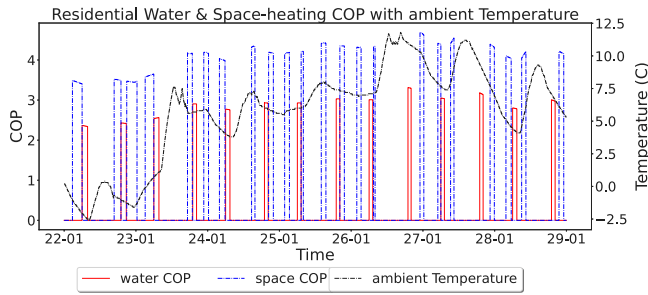$$COP(t) = 7.90471e^{-0.024(T_{ret}(t) - T_a(t))} \quad (18)$$

Fig. 6. Simulation example of a week of residential Space-Heating and DHW COPs and ambient Temperature during Winter.
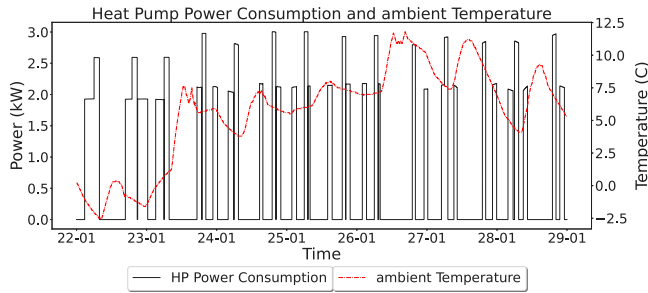

Fig. 7. Simulation example of a week of residential HP power consumption and ambient temperature during winter.

$$\dot{Q}_{hp}(t) = \dot{m}_{wat}C_{wat}(T_{sup} - T_{ret}(t))$$
$$\leftrightarrow T_{ret}(t) = T_{sup} - \frac{\dot{Q}_{hp}(t)}{\dot{m}_{wat}C_{wat}} \tag{19}$$

Finally, the power consumption model is modeled in (17)–(19). The HP power consumption P_{hp} depends on the HP heating output $\dot{Q}_{hp}$ and the Coefficient of Performance (COP). The latter is estimated by regression from 10 different HP models in [27] and is dictated by (18). Finally, (19) models the HP output, which depends on the water flow rate $\dot{m}_{wat}$, the water-specific heating capacity C_{wat} and the difference of the supply and return water temperature, T_{sup} & T_{ret}, respectively.

The considered HP in this work is an ON-OFF reversible Air-Sourced Heat Pump (ASHP), which uses floor heating for space heating. The specifications, such as the HP heating output, have been acquired by the Dimplex LIK 8MER module [28], which has a rated flow water rate $\dot{m}_{wat} = 0.8$ m³/h and uses supply temperatures T_{sup} of 35 °C, 50 °C & 18 °C for floor-heating, DHW & floor-cooling, respectively. The heating model represents a temperature controller, which keeps the building temperature within the desired interval [21°, 23°] as long as the building is occupied. In this regard, the buildings have been considered to be empty during 8:00–14:00 on weekdays. Moreover, the use of DHW has been considered once per day, every day at 6:00, which then is always prioritized against space heating.

In Figs. 6 and 7, key results of the heating model for a Winter week are summarized. As it can be observed in Fig. 6, the space-heating COPs are always higher than the DHW COPs, reaching up to the value of 4.2. This is due to the lower heating temperature, that is used for the floor heating, because the COP always depends on the difference of the source and sink temperatures. This also can be seen, by observing the trend of both COPs during ambient temperature increases. Finally, Fig. 7 depicts the HP power consumption versus the ambient Temperature during the same week. Due to the different COPs, the low consumption pulses are related to the space-heating, while the high pulses belong to the DHW. The average consumption for space-heating fluctuates around 2 kW, while it can reach approximately up to

Table 2
Tank, building & HP parameters.

Parameters	Explanation	Value
C_b	Building Capacity	4.755 kWh/K
V_b	Building Volume	585 m³
C_{air}	Air Spec. Capacity	0.279 Wh/kgK
ρ_{air}	Air Density	1.225 kg/m³
$\dot{m}_{wat}$	HP Flow Water Rate	0.8 kg/s
C_{wat}	Water Spec. Capacity	1.16 Wh/kgK
w_b	Window-to-Wall Ratio	0.3
s_b	Solar Heat Gain Coef.	0.2
r_b	Air Change Rate	0.35 h⁻¹
V_{tank}	Tank Volume	215 m³
U_{tank}	Tank Conductivity	0.598 W/m²K
A_{tank}	Tank Total Area	2.21 m²

3 kW for DHW use. The tank, building & HP parameters are summarized in Table 2.

2.5. Indicators for assessing the PV system performance

To quantify the percentage of solar power that is directly used by the traction and residential loads, the authors define the **Direct PV Utilization** factor, U_{PV}, as in [7,8]:

$$U_{PV} \triangleq \frac{\int_{year}(P_{load} - P_{grid})\,dt}{\int_{year}P_{PV}dt} \tag{20}$$

With P_{load} the total load power demand at the substation (trolleybuses and households), P_{grid} the power delivered from the AC grid, and P_{PV} the PV generated power is the power demanded from or sent to the grid by the SS with a solar PV system. the **Direct Load Coverage**, Λ, is the fraction of the load that the output of the PV system can directly supply, and it can be expressed by:

$$\Lambda \triangleq \frac{\int_{year}(P_{load} - P_{grid})\,dt}{\int_{year}P_{load}\,dt} \tag{21}$$

Finally, for a normalized sizing nomenclature of the PV system, the **Energy-Neutrality Ratio**, ζ, is defined as in [7,8]:

$$\zeta \triangleq \frac{\int_{year}P_{PV}dt}{\int_{year}P_{load}dt} \tag{22}$$

In simpler words, a $\zeta = 1$, means a PV system size whose net PV generation over a year is equal to that of the substation energy demand (net energy neutral).

3. Results: Benefits in direct PV utilization

As mentioned earlier, households can reduce the PV curtailment by providing the load demand in the frequent moments of zero or low load demands at traction substations. This can be illustrated in the one-hour extract of the PV system performance at SS12 in Fig. 8. The figure compares two systems of the same size: A single traction stakeholder and a shared stakeholder system between the traction substation and 15 households.

The PV generation is almost fully utilized (100% U_{PV}) at numerous instances in the combined system. Meanwhile, utilization of up to 80% is ensured when the single stakeholder system is in full-curtailment mode (no bus demand).

These results are further discussed in this section.

3.1. Case of a long, low traffic substation

Fig. 9(a) shows the PV system utilization, U_{PV}, at a long yet low traffic traction substation. With increasing PV system sizes, U_{PV} is lower as the mismatch between the generation and load is higher.
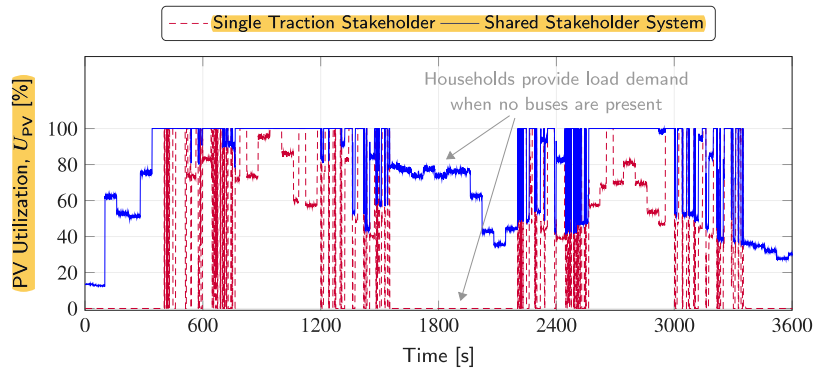
Fig. 8. Comparison of the PV Utilization between the single and combined stakeholder systems (one-hour excerpt of a July day at Substation 12 without or with 15 households).
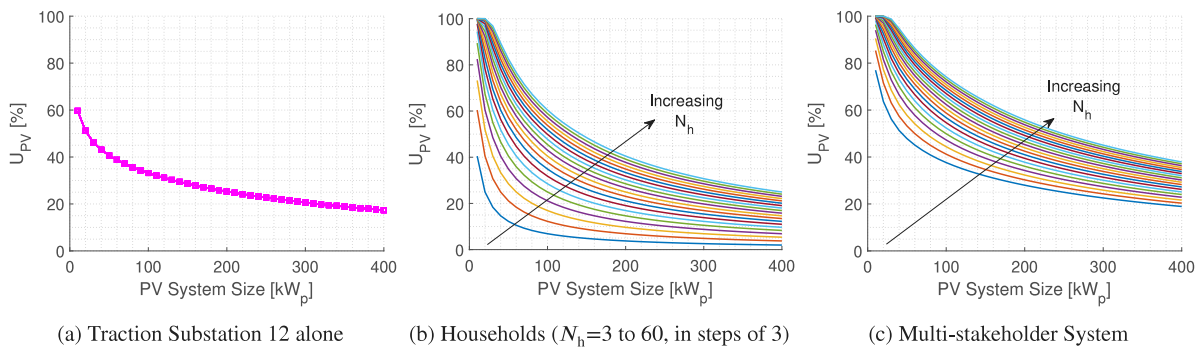

Fig. 9. Benefit in direct PV utilization, U_{PV}, for the individual stakeholders and the shared system for a Long, Low Traffic substation in a one-year simulation.

The knee of the curve can be seen at about 40 kW, which is the value of the bus auxiliaries and, therefore, constitutes a sort of "base load" for the traction substation power demand when and if a bus is present on the section. For systems lower than this knee value, U_{PV} rapidly increases as such small PV systems generate powers that are consumed almost in full when and if a bus is present on the section. This "when and if" condition dictated by the timetabling is the reason the U_{PV} does not reach 100%. However, smaller system sizes are not particularly attractive as they do not cover a large part of the traction load.

For substation 12, the net energy-neutral PV system size ($\zeta = 1$) is 195 kW and of a U_{PV} of 25.6%. Consequently, 74.4% of the PV generation needs to be stored, exchanged with the AC grid, and/or curtailed. Fig. 10(b) shows the U_{PV} for different numbers of connected households, N_h. The curves go from 3 to 60 houses, in steps of 3, to represent each of the 3 available household profiles of Fig. 5.

Fig. 9(c) shows the increase in the U_{PV} when the PV system serves a combined traction-residential load. In this case, the energy-neutral PV system of 195 kW is at about 29% in U_{PV}, creating a net reduction in generation mismatch of absolute 3.4 percentage points. Obviously, this PV system is now covering more loads, and therefore, this system size is no longer considered "energy neutral" for the combined load. The effect on the load coverage is discussed in the following section of this paper. However, the key takeaway from the U_{PV} analysis is the observable net jump in the utilization curves when comparing Figs. 9(a) and 10(b) to Fig. 9. The values in the latter figure reach, in many cases, up to 100% utilization, which argues that the benefits of this shared system are not otherwise reachable by a simple under-sizing of the PV system in the single-stakeholder cases.

3.2. Case of a short, high traffic substation

The results of Substation 9, in Fig. 10, validate the previous results and conclusions of Substation 12.

For this substation, despite the high traffic that the substation experiences, a consequence of its short supply zone length is that it does not have many bus and traffic-light stops. Furthermore, the buses could enter and exit the section without activated auxiliaries (mainly heating/cooling). This leaves the U_{PV} with a similar knee around 40 kW, yet smaller system sizes do not bring the accelerated increase observed in long-supply-zones substations as seen in Fig. 10(a).

However, Fig. 10(c) shows the same positive jump in the U_{PV} curves as seen in the case of long, low-traffic substations with values above the curves of both Figs. 9(b) and 10(a).

4. Results: Benefits in load coverage

The PV system utilization was shown to have a positive effect at both low and high-traffic substations when sharing their PV system with any number of households. However, it is still important to study the individual traction load coverage of these shared PV systems to ensure that this benefit does not effectively come from an implicit under-sizing approach since the PV system now serves more load demand.

In that aim, Fig. 11 shows the load coverage of the individual traction and residential systems. From an energy perspective, the share of each stakeholder in the PV system can be established from the energy it utilized over a year. This can be used to define an *effective* PV system size for each stakeholder to help quantify the benefit of the shared system.

For example, it is deduced from the simulations that a 200kWp (kW peak) PV system connected to SS 12 and 3 neighboring households delivers directly 80% of its power to the traction substation over the year and 20% to the households. This *effectively* means that the energy that the traction substation receives is *equivalent* to having installed an 80kWp system. However, the simulations show that an 80kWp system would give SS12 about 1% less direct load coverage than an 80% share of a 100kWp multi-stakeholder system. This validates first the claim
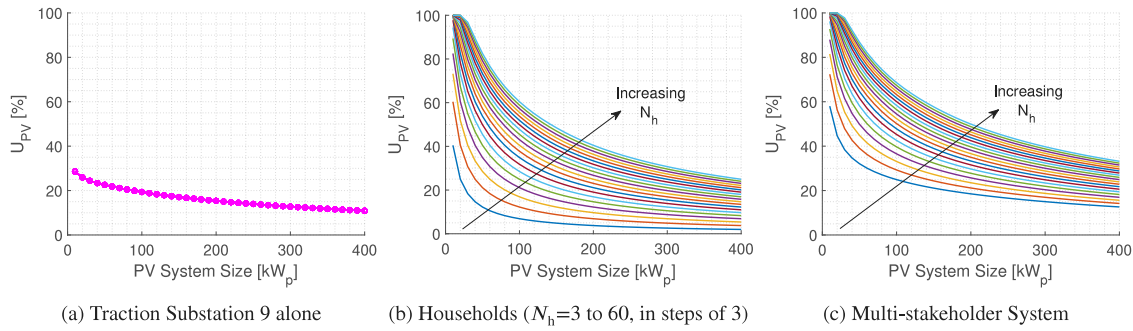
(a) Traction Substation 9 alone (b) Households (N_h=3 to 60, in steps of 3) (c) Multi-stakeholder System

Fig. 10. Benefit in direct PV utilization, U_{PV}, for the individual stakeholders and the shared system for a Short, High Traffic substation in a one-year simulation.
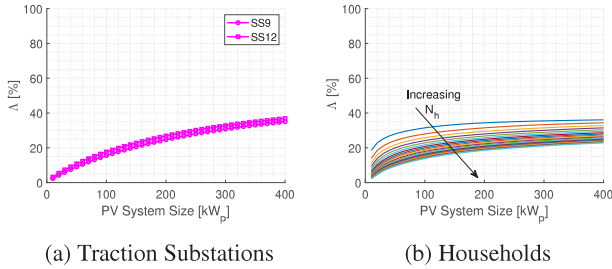

(a) Traction Substations (b) Households

Fig. 11. Direct Load Coverage by a PV system connecting only to a traction substation or to households.

(a) Effective PV System size (b) Load Coverage Comparison

Fig. 12. Effective PV System size based on the share of output consumed from the installed PV system (left) and the increase in load coverage compared to a single-stakeholder system of that effective size (right) for Substation 12.

(a) Effective PV System size (b) Load Coverage Comparison

Fig. 13. Effective PV System size based on the share of output consumed from the installed PV system (left) and the increase in load coverage compared to a single-stakeholder system of that effective size (right) for Substation 9.

that the benefit in utilization is not the consequence of an implicit undersizing and second that the combined system offers better coverage per kWp installed than a single-stakeholder system. These results for all PV system sizes and household numbers are presented in Fig. 12(a) and Fig. 12(b), respectively. Since none of the curves in these figures cross below the zero value, it can be concluded that there is always a net benefit on the load coverage from a combined system that goes hand in hand with a net benefit in direct utilization. The energy-neutral system of 198 kW for this substation ($\zeta = 1$) can be traced in Fig. 12(b) to an increase of about 5 percentage points.

This means that a shared, multi-stakeholder system offers less of a need for storage, curtailment, and grid exchange, as well as a net benefit in the direct load coverage (kWh delivered) per installed capacity (kWp installed).

These results are also valid for the short, high-traffic substation SS9, as can in Fig. 13. The energy-neutral system of 129 kW for this substation ($\zeta = 1$) can be traced in Fig. 13(b) to an increase of about 6–7 percentage points. While the net percentage point benefit is seen above 10% for large system sizes, it is important to remember that this substation has an energy-neutral system size of 129 kW rather than the 198 kW of SS12. In that regard, a 400kWp system is relatively much larger for this substation than other substations and would directly cover significantly more of the load, yet at the expense of a lower PV utilization.

5. Conclusions and recommendations

This paper looked at a multi-stakeholder PV system shared between traction substations and nearby residential dwellings. In the shared system, the residential demand is expected to provide a base load to the PV system, while the traction demand provides peak demand periods. Together, this would offer a better matching of generation and load and make the system more techno-economically feasible by reducing the need for storage, AC grid exchange, and curtailment. Moreover, rooftop PV systems would offer the traction substations the otherwise-scarce urban space to install the PV panels.
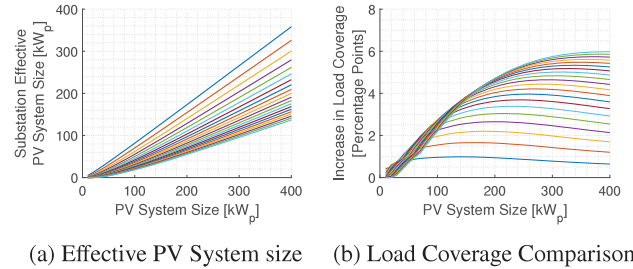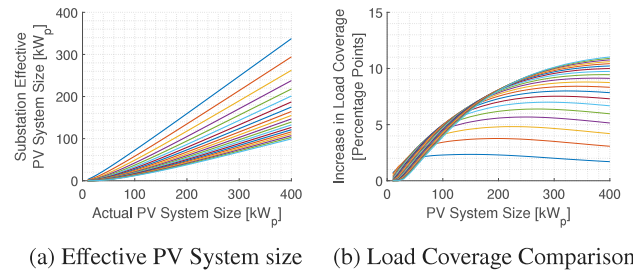
In terms of the direct PV utilization, U_{PV}, there was a positive benefit in combining any traction substation with any number of households.

This benefit is shown to be an intrinsic benefit of the shared system and not an implicit consequence of the effective undersizing of the PV system, as it now delivers two load demands.

Furthermore, the shared PV system is shown to deliver more direct energy to the loads per effective kWp installed. Here, there was also a positive benefit for any combination of traction substations and households. This meant that the return on the investment in a share of a combined system brings more load coverage than having installed a dedicated PV system to one stakeholder of the size of that share.

Future works are urged to look at an optimal sizing approach to the number of connected households and PV system size at a traction substation with respect to costs, physical space available, and the use of storage.

CRediT authorship contribution statement

Ibrahim Diab: Writing – review & editing, Writing – original draft, Visualization, Validation, Methodology, Investigation, Formal analysis, Data curation, Conceptualization. **Nikolaos Damianakis:** Writing

– review & editing, Writing – original draft, Visualization, Validation, Investigation, Formal analysis, Data curation. **Gautham Ram Chandra-Mouli:** Writing – review & editing, Writing – original draft, Validation, Supervision, Funding acquisition. **Pavol Bauer:** Writing – review & editing, Writing – original draft, Validation, Supervision, Funding acquisition.

Declaration of competing interest

The authors declare that they have no known competing financial interests or personal relationships that could have appeared to influence the work reported in this paper.

Data availability

Data will be made available on request.

Acknowledgments

References

[1] IEA. Approximately 100 million households rely on rooftop solar PV by 2030 – Analysis. 2022, https://www.iea.org/reports/approximately-100-million-households. [Accessed 22 March 2023].

[2] Diab I, Chandra Mouli GR, Bauer P. Toward a better estimation of the charging corridor length of in-motion-charging trolleybuses. In: 2022 IEEE transportation electrification conference & expo. 2022, p. 557–62.

[3] Diab I, Eggermont R, Mouli GRC, Bauer P. An adaptive battery charging method for the electrification of diesel or CNG buses as in-motion-charging trolleybuses. IEEE Trans Trans Electrif 2023;1, doi10.1109/TTE.2023.3243022.

[4] Diab I, Saffirio A, Chandra Mouli GR, Singh Tomar A, Bauer P. A complete DC trolleybus grid model with bilateral connections, feeder cables, and bus auxiliaries. IEEE Trans Intell Transp Syst 2022;1–12.

[5] Bartłomiejczyk M. Dynamic charging of electric buses. Gdańsk University of Technoligy, Faculty of Electrical and Control Engineering; 2018, URL https://books.google.cz/books?id=ziX_vQEACAAJ.

[6] Vanhool. A bus for the future, Leipzig, October, 2012. 2012, [Online]. http://www.trolley-project.eu/fileadmin/user_upload/download/Summit/TROLLEY_2nd_Summit_Jenne_ABusForTheFuture.pdf. [Accessed 23 February 2018].

[7] Diab I, Scheurwater B, Saffirio A, Chandra-Mouli GR, Bauer P. Placement and sizing of solar PV and Wind systems in trolleybus grids. J Clean Prod 2022;131533.

[8] Diab I, Saffirio A, Chandra-Mouli GR, Bauer P. A simple method for sizing and estimating the performance of PV systems in trolleybus grids. J Clean Prod 2023;384:135623.

[9] Diab I, Mouli GRC, Bauer P. A review of the key technical and non-technical challenges for sustainable transportation electrification: A case for urban catenary buses. In: 2022 IEEE 20th international power electronics and motion control conference. IEEE; 2022, p. 439–48.

[10] Wołek M, Wolański M, Bartłomiejczyk M, Wyszomirski O, Grzelec K, Hebel K. Ensuring sustainable development of urban public transport: A case study of the trolleybus system in Gdynia and Sopot (Poland). J Clean Prod 2021;279:123807.

[11] Diab I, Mouli GRC, Bauer P. Increasing the integration potential of EV chargers in DC trolleygrids: A bilateral substation-voltage tuning approach. In: 2022 International symposium on power electronics, electrical drives, automation and motion. 2022, p. 264–9.

[12] Bartłomiejczyk M, Jarzebowicz L, Hrbáč R. Application of traction supply system for charging electric cars. Energies 2022;15(4):1448.

[13] van der Horst K, Diab I, Mouli GRC, Bauer P. Methods for increasing the potential of integration of EV chargers into the DC catenary of electric transport grids: A trolleygrid case study. eTransportation 2023;100271.

[14] Asare-Bediako B, Kling W, Ribeiro P. Future residential load profiles: Scenario-based analysis of high penetration of heavy loads and distributed generation. Energy Build 2014;75:228–38, URL https://www.sciencedirect.com/science/article/pii/S037877881400139X.

[15] Gupta R, Pena-Bello A, Streicher KN, Roduner C, Farhat Y, Thöni D, et al. Spatial analysis of distribution grid capacity and costs to enable massive deployment of PV, electric mobility and electric heating. Appl Energy 2021;287:116504, URL https://www.sciencedirect.com/science/article/pii/S0306261921000623.

[16] Langer L, Volling T. An optimal home energy management system for modulating heat pumps and photovoltaic systems. Appl Energy 2020;278:115661, URL https://www.sciencedirect.com/science/article/pii/S0306261920311570.

[17] Wei W, Gu C, Huo D, Le Blond S, Yan X. Optimal borehole energy storage charging strategy in a low carbon space heat system. IEEE Access 2018;6:76176–86.

[18] UITP. The road to sustainability: transition to renewable energy in public transport. uitp.org.

[19] Tomar AS, Veenhuizen B, Buning L, Pyman B. Estimation of the size of the battery for hybrid electric trolley busses using backward quasi-static modelling. In: Multidisciplinary Digital Publishing Institute proceedings. Vol. 2. No. 23. 2018, p. 1499.

[20] KNMI. Meteorological data downloaded with Meteonorm. 2019.

[21] Karasu S, Altan A. Recognition model for solar radiation time series based on random forest with feature selection approach. In: 2019 11th International conference on electrical and electronics engineering. 2019, p. 8–11.

[22] Hacioğlu R. Prediction of solar radiation based on machine learning methods. J Cogn Syst 2017;2(1):16–20.

[23] Smets AH, Jäger K, Isabella O, van Swaaij R, Zeman M. Solar energy: The physics and engineering of photovoltaic conversion technologies and systems. UIT; 2016.

[24] Centraal Bureau voor de Statistiek. Energy consumption private dwellings by type of dwelling and regions. 2016, URL http://statline.cbs.nl/StatWeb/publication.

[25] Vereniging Nederlandse Energie- Data Uitwisseling (NEDU). http://nedu.nl.

[26] Damianakis N, Mouli GCR, Bauer P. Risk-averse estimation of electric heat pump power consumption. In: 2023 IEEE 17th international conference on compatibility, power electronics and power engineering. IEEE; 2023, p. 1–6.

[27] Oliyide RO, Cipcigan LM. The impacts of electric vehicles and heat pumps load profiles on low voltage distribution networks in Great Britain by 2050. Int Multidiscip Res J 2021;11:30–45.

[28] Dimplex. Project planning manual heating and cooling with heat pumps. 2008, Dimplex. URL https://www.dimplex-partner.de/fileadmin/dimplex/downloads/planungshandbuecher/en.